Published in final edited form as:
Neuron. 2012 June 7; 74(5): 899–910. doi:10.1016/j.neuron.2012.04.014.

Spontaneous high-gamma band activity reflects functional organization of auditory cortex in the awake macaque

Makoto Fukushima, **Richard C. Saunders**, **David A. Leopold**, **Mortimer Mishkin**, and **Bruno B. Averbeck**
Laboratory of Neuropsychology, National Institute of Mental Health, National Institutes of Health, Bethesda, Maryland 20892, U.S.A

Summary

In the absence of sensory stimuli, spontaneous activity in the brain has been shown to exhibit organization at multiple spatiotemporal scales. In the macaque auditory cortex, responses to acoustic stimuli are tonotopically organized within multiple, adjacent frequency maps aligned in a caudorostral direction on the supratemporal plane (STP) of the lateral sulcus. Here we used chronic micro-electrocorticography to investigate the correspondence between sensory maps and spontaneous neural fluctuations in the auditory cortex. We first mapped tonotopic organization across 96 electrodes spanning approximately two centimeters along the primary and higher auditory cortex. In separate sessions we then observed that spontaneous activity at the same sites exhibited spatial covariation that reflected the tonotopic map of the STP. This observation demonstrates a close relationship between functional organization and spontaneous neural activity in the sensory cortex of the awake monkey.

Introduction

Converging evidence from neurophysiology and from functional and metabolic neuroimaging demonstrate that the brain is continually active in the absence of sensory inputs or motor tasks (Kennedy et al., 1978; Arieli et al., 1995; Biswal et al., 1995; Raichle et al., 2001). There has recently been considerable interest in whether this spontaneous activity reflects, and can be used to investigate, the underlying architecture of the functional networks within the brain. Neurophysiological evidence for this prospect comes, for example, from experiments using optical imaging of voltage sensitive dyes, which have shown that the correlation structure of spontaneous activity in visual cortex reflects the spatial structure of an orientation map derived from sensory stimulation (Kenet et al., 2003). A recent fMRI study has similarly shown correspondence between spontaneous signals and the functional organization of the somatosensory cortex (Chen et al., 2011). Moreover, studies with single unit electrophysiology have demonstrated that there is a higher level of correlation in spontaneous spiking activity between pairs of neurons that have similar tuning properties (Lee et al., 1998; Crowe et al., 2010). Furthermore, the spontaneous activity of single neurons can reflect the global state of the network in which they are embedded (Arieli et al., 1996; Tsodyks et al., 1999; Luczak et al., 2009). In summary, the brain's endogenous

Contact Information: Makoto Fukushima, Laboratory of Neuropsychology, National Institute of Mental Health, National Institutes of Health, Building 49, Room 1B80, 49 Convent Drive, Bethesda, MD 20892, makoto_fukushima@me.com, Phone: +1-301-443-7458.

activity can exhibit significant spatial and temporal structure, and this structure can be related to the underlying functional properties of the network.

At the same time, it is unclear to what extent previous observations reflect a general principle of cortical function. Most of the imaging studies in visual and somatosensory cortex mentioned above were conducted in anesthetized rodents and cat, but the anesthesia or behavioral state can influence spontaneous neural activity. In humans the correlation structure of gamma-band spontaneous-activity in the awake state is different from that in slow-wave sleep (He et al., 2008). It is therefore important to establish whether there is a correspondence between spontaneous activity and functional architecture in awake primates. Furthermore, the focus of previous studies was on the spatial organization within a single cortical area over a few millimeters. Would a similar correspondence occur over a larger cortical distance and multiple areas in the awake monkey? A previous study using an array of multielectrodes in early visual cortex of awake monkeys found that correlation in spontaneous activity fell off monotonically with distance, up to a centimeter, but made no attempt to link the ongoing spontaneous activity within that area to the intrinsic functional architecture (Leopold et al., 2003; Leopold and Logothetis, 2003).

In the present study, we address the spatial organization of spontaneous field-potential signals in the core and surrounding regions of the macaque auditory cortex using multiple micro-electrocorticographic (μECoG) arrays with finer spacing between sites (1 mm) than that of standard ECoG grids (Kim et al., 2007; Kellis et al., 2010). The arrays were placed along the length of the supratemporal plane (STP) in the lateral sulcus (Figure 1B and C) where there are multiple tonotopic maps (Merzenich and Brugge, 1973; Morel et al., 1993; Recanzone et al., 2000; Petkov et al., 2006; Tanji et al., 2010). Three of the μECoG arrays were placed end-to-end, running more than 2 cm in the caudorostral direction, and thus spanning multiple auditory areas (Figure 1C; note that this figure is reconstructed from the postmortem brain after removing the upper bank of the lateral sulcus following all the data collection). This approach allowed us to first identify the tonotopic maps based on field potential responses to pure tone acoustic stimuli, and to then compare these maps to the correlation structure of spontaneous activity recorded in separate sessions. Thus, we tested the hypothesis that the spontaneous activity reflects the functional architecture of the sensory map as previously shown in anesthetized animals (Kenet et al., 2003). We found that the dominant eigenmodes of the correlation patterns closely resembled the stimulus-defined functional map, suggesting that the pattern of spontaneous activity was constrained by the large-scale functional architecture of the STP. As the first such demonstration in awake monkeys, these findings underscore the close link between the spatiotemporal structure of the brain's endogenous activity and the functional organization within and between cortical areas.

Results

The tonotopic organization of the auditory cortex in awake macaques is known from previous single-unit (Recanzone et al., 2000; Kusmierek and Rauschecker, 2009; Scott et al., 2011) and fMRI (Petkov et al., 2006; Baumann et al., 2010; Tanji et al., 2010) studies. Moreover, the frequency tuning properties in the auditory cortex have been evaluated using local field potential (LFP) recordings and current source density (CSD) analysis (Fu, 2004; Lakatos et al., 2005a; Kayser et al., 2007; Steinschneider et al., 2008; Kajikawa and Schroeder, 2011). The tonotopic maps run in a caudorostral direction and show mirror reversals in their preferred frequency gradient at the points of their lowest and highest frequencies. With three chronically implanted μECoG arrays (total 96 channels, Figure 1B, C), we were able to characterize these multiple maps simultaneously by measuring responses to each stimulus presentation. We were also able to measure spontaneous activity

from the same cortical positions in a separate testing session. Furthermore, the simultaneous recording with chronic μECoG arrays permitted the analysis of spatiotemporal covariation in the spontaneous field potentials. In the following sections we first describe the methods that identified the tonotopic maps in the auditory cortex and then demonstrate that spontaneous activity is organized in a manner that reflects the specific structure of these maps.

Tonotopic mapping of the STP derived from high-gamma power in field potentials

We recorded auditory evoked potentials from the implanted μECoG arrays while the monkeys listened passively to 180 different pure tone stimuli (each 100 ms duration, at 30 different frequencies from 100 Hz to 20 kHz at each of 6 intensity levels from 52–87 dB; see Experimental Procedures). The tone stimuli evoked robust responses (Figure 2). Unlike the average evoked waveform, which was dominated by the lower frequency components phase-locked to stimulus onset (Figure 2A, lower panels), the normalized spectrogram clearly shows increases from the pre-stimulus period in higher frequency power, especially in the high-gamma range (60–250 Hz) (Figure 2A, upper panels) possibly due to the fact that the spectrogram reflects not only phase-locked but also nonphase-locked components of the evoked response.

To evaluate the auditory frequency preferences of individual sites, we estimated the characteristic frequency (CF) for each site based on the evoked high-gamma power from the first 150 ms after the presentation of the stimulus (see Experimental Procedures). This produced tuning profiles with clear frequency preferences, which sometimes became better defined at lower sound intensities (Figure 2B, left; see also Figure S3), but could also be relatively independent of sound intensity (Figure 2B, right). The statistical significance of this frequency preference was evaluated using a two-way analysis of variance (ANOVA, $p < 0.01$; see Experimental Procedures). About two-thirds of the sites in STP showed significant frequency tuning (65/96 sites in Monkey M, 62/96 sites in Monkey B), and were organized in a tonotopic fashion, with CF reversals (Figure 3). The maps were similar in the two monkeys. Starting at the most caudal electrodes in the caudal-most array, sites were tuned to comparatively high frequencies. Moving rostrally along the STP, the frequency tuning went through at least three well-defined reversals over a distance of roughly 2 cm. As the CF changed primarily along the caudorostral axis, we projected the CF from each site onto this axis to discern the areal boundaries defined by the frequency reversals (Figure 3B). We then fit the data with a polynomial (dashed curve in Figure 3B; see Experimental Procedures,) and used its peaks and troughs to determine the approximate locations of the boundaries between adjacent cortical areas. Based on this analysis, we conceptually divided the recording sites on STP into four sectors, which we estimate correspond to the following subdivisions within the auditory cortex: Sec (Sector) 1: A1/ML; Sec 2: R/RL; Sec 3: RTL; Sec 4: RTp (Figure 3A). The core/belt (e.g. A1/ML) boundary within Sec 1 or Sec 2 could not be determined by changes in the CF because the tuning frequency does not vary along the medial-lateral axis of the STP (e.g. Petkov et al., 2006). Nor could we detect the boundary with any certainty based on differences in sharpness or strength of tuning between the belt and the core (Rauschecker et al., 1995).

We also examined maps obtained with other field potential frequency bands. Although the CF maps from the lower frequency bands (theta, alpha, beta, and low-gamma) were similar to the map from the high-gamma band (Figure S1), it was more difficult to discern clear reversals in the CF maps from the lower frequency bands. The difficulty is evident from inspection of the CF values projected on the caudorostral axis of the supratemporal plane (Fig. S1A, B, right column). In the lower frequency bands, the CF values did not vary and reverse as smoothly as those in the high-gamma band. To quantify the difference, we examined how well a polynomial curve fit each of the CF maps projected on the

caudorostral axis (the blue curves in the columns on the right in Figure S1A and B). We found that high-gamma had the highest R^2. Although high R^2 values could be obtained from untuned data (i.e. without frequency tuning, all points could lie on a line and still be well fitted), it is clear from the plots that the drop in the value of R^2 for the other evoked frequency bands was due to decreased consistency in tuning along the caudorostral axis. The results indicate not only that the high-gamma band produced the clearest tonotopic maps, but also that the other frequency bands produced noisier, although consistent maps. To test this point further, we also examined the optimal degree of polynomials fit to the CFs using the Bayesian Information Criteria (BIC) (see Supplemental Experimental Procedures). The maps from the low frequency bands were fitted optimally with 1st or 2nd order polynomials (Table S2: theta and beta bands in Monkey M; theta, alpha, beta, and low-gamma bands in Monkey B, see Supplemental Experimental Procedure), suggesting that the data from these frequency bands were not structured enough to have the multiple mirror symmetric reversals evident in data from the highest frequency band. In Monkey M, the data from the alpha and low-gamma band were best fitted with higher order polynomials (9 for alpha band, 7 for low-gamma), but high-gamma was the only frequency band optimally fitted by the structured polynomial curve in both monkeys (10 for Monkey M, 7 for Monkey B).

Spontaneous neural fluctuation reflects the structures of the tonotopic map

Given the well-defined tonotopic maps obtained with high-gamma-band evoked powers, we next investigated the spatiotemporal structure of spontaneous neural activity, asking whether fluctuations of high-gamma activity in the auditory cortex might reflect its inherent functional architecture. In this case, we recorded field potentials from the arrays while the monkeys sat quietly with no auditory stimulus (see Experimental Procedures). First we examined individual time frames of the high-gamma-band voltage to determine whether they would exhibit structural similarities to the CF maps. We found that some individual time frames bore a resemblance to the maps (Figure 4A). To determine whether such similarity was coincidental or systematic, we computed the correlation coefficient between the spatial distribution of spontaneous high-gamma voltage at each time frame and the CF map for each monkey. As a control, we computed the correlation coefficient between the spontaneous activity and spatially randomized CF maps (see Experimental Procedures). The distribution of the correlation coefficient from the actual CF map (red, Figure 4B) was significantly different from the control distribution (black, Figure 4B) (Kolmogorov-Smirnov test, $p < 0.0001$ for both monkeys). The tails of the distribution are wider than the control distribution, and thus these tails include correlation coefficients that are significantly larger (two-tailed) than would be expected from the control distribution. Statistically significant correlation coefficients were then defined by fitting the control distribution with a Gaussian and calculating the correlation coefficients satisfying $p < 0.01$ (two sided). Under this definition, the threshold for significant correlation was ±0.305 for Monkey M and ±0.307 for Monkey B (gray area, Figure 4B). The time frames above those thresholds occupy 10.6% and 7.7% for Monkeys M and B, respectively, of all the recorded spontaneous frames, demonstrating that during certain periods the spontaneous raw voltage reflected the structure of auditory cortex over multiple areas.

To examine this issue in greater depth, we next evaluated whether the spontaneous activity resembling the CF map described above explains a large or small fraction of the overall spontaneous activity variance. To this end, it was necessary to extract the dominant spatial structure present in the ongoing spontaneous activity without using the information about the CF map. Thus, we estimated the extent to which the activities of individual electrodes were coordinated by computing the principal components (PCs) of the spontaneous high-gamma voltage in the 96 sites on the STP (see Experimental Procedures). We found that the amount of variance explained by each PC decreased rapidly from the first PC, which

suggests that the spontaneous activity was strongly coordinated according to its spatial organization (Figure 5). Specifically, 80% of the variance was explained by the first 22 PCs for Monkey M and the first 32 PCs for Monkey B), while the first 77 PCs would be necessary to explain 80% of the variance with uniformly distributed eigenvalues. Thus, there was considerable structure in the spontaneous activity.

Inspection of the PCs demonstrated a notable correspondence between several of the PCs computed using spontaneous activity and the CF map of pure-tone responses (compare, for example, Figure 6B and Figure 3A). Therefore, we statistically evaluated whether each PC was correlated with either or both of the two variables that characterize each site, i.e. the CF and the area label (i.e. Sector 1, 2, 3, 4) (see Experimental Procedures). We found that both monkeys had multiple PCs with significant ($p < 0.05/96$) main effects for the CF and/or the area label (Table S3). Interestingly, the PCs that were significantly correlated with the features of the map also explained the most variance in the spontaneous activity. Specifically, the first PCs in both monkeys were significantly correlated with the area label. In addition, for each monkey, the highest-order PC that correlated with the CF map also ranked highly (second PC for Monkey M, fourth PC for Monkey B). By examining the PCs spatially, one can readily see that the first PCs resembled our stimulation-based estimation of the different auditory areas (Figure 6A). The other PCs closely resembled the CF maps themselves (Figure 6B). We also confirmed the relationship between the CF values and these PCs by calculating the correlation coefficients between them for both monkeys: $r = 0.5243$ ($p < 0.00001$) for Monkey M; $r = 0.3858$ ($p = 0.0023$) for Monkey B (Figure 6C).

Discussion

In this study, we chronically implanted μECoG arrays to record field potentials in intrasulcal auditory cortex of awake macaques. Based upon the responses to pure tone stimuli, and consistent with previous electrophysiological and fMRI studies, we first identified multiple, mirror symmetric tonotopic maps on the supratemporal plane (STP) using the high-gamma band of the evoked field potentials. We then demonstrated that, in the absence of stimulation, spontaneous activity on the STP was spatiotemporally coordinated in a way that reflected two functional organizations of the auditory cortex: the characteristic frequency (CF) maps and the sectors delineated by the putative areal boundaries from the CF maps. In the next sections we discuss each of these aspects of the study in turn, and speculate on the significance of the emergent spontaneous activity patterns.

Tonotopic organization of field potentials of the supratemporal plane revealed by μECoG arrays

As in humans, the core and belt areas of the auditory cortex of the macaque monkey are embedded in the lateral sulcus on the STP, with additional auditory areas located along the lateral bank of the circular sulcus and on the superior temporal gyrus (Bolhuis et al., 2010; Hackett, 2011). Traditionally, sensory responses from such intrasulcal areas have been investigated with single or multiple penetrating electrodes by recording extracellular spikes and field potentials. In the macaque auditory cortex, these direct measurements have revealed detailed aspects of the sound encoding properties within various frequency bands of the field potentials (Lakatos et al., 2005a; Chandrasekaran and Ghazanfar, 2008; Steinschneider et al., 2008; Kayser et al., 2009; Fishman and Steinschneider, 2010). This approach, however, is not well suited to examining spatiotemporal activation profiles from a large expanse of the cortex. Optical imaging of voltage sensitive dyes has revealed spatiotemporal activation patterns in sensory cortex (Huang et al., 2004; Xu et al., 2007; Wu et al., 2008), but this method cannot measure neural activity from intrasulcal cortical areas such as the STP. On the other hand, fMRI can probe the entire brain simultaneously, but it has low temporal resolution. In the present study, we circumvented these limitations by

adopting intracranial micro-electrocorticography (μECoG). The μECoG arrays used in the current study had finer spacing between sites (1 mm) than that of standard ECoG grids. This approach allowed us to extract the fine tonotopic representation in the macaque auditory cortex on the STP in the lateral sulcus at high temporal resolution.

Mirror symmetric tonotopic maps that reverse at areal boundaries in auditory cortex are one of the main features shared by many primate species, including humans (Formisano et al., 2003; Da Costa et al., 2011; Hackett, 2011). In awake macaques, tonotopic maps have been identified using single-unit recordings (Recanzone et al., 2000; Kusmierek and Rauschecker, 2009; Scott et al., 2011), but maps have not been identified in far rostral sites on the STP, and, in fact, there are only a few studies that have recorded single units from rostral areas (Kikuchi et al., 2010; Perrodin et al., 2011). In the current study, we identified mirror symmetric tonotopic maps from primary to rostral areas, using the high-gamma power of the evoked field potential. Previous studies have shown that in the macaque primary auditory cortex tuning curves for stimulus frequency obtained from multi-unit spiking activity were better correlated with high-gamma power in local field potentials (LFPs) than with power in the lower frequency components of the LFP (Kayser et al., 2007). Previous studies in other cortical sensory areas have similarly demonstrated that spiking activity has a closer relation to high-gamma power than to power in lower frequencies (Liu and Newsome, 2006; Ray et al., 2008). These studies suggest that the tonotopic maps obtained from high-gamma band power in our data reflect spiking activity in the vicinity of each contact, presumably from upper layers of cortex since the μECoG arrays were placed on the cortical surface. A recent study of rat auditory cortex showed better correlation between stimulus-evoked spikes and high-gamma-band CSD amplitude from the supragranular layer than from deeper layers (Ogawa et al., 2011). This trend was shared by stimulus evoked and pre-stimulus spontaneous activity, although the stimulus evoked responses generally had higher correlation between the CSD amplitudes and neuronal fringing for all bands than did the pre-stimulus spontaneous activity (Ogawa et al., 2011). The phase dependency of neuronal firing, on the other hand, may not depend on the frequency bands of the field potential in spontaneous activity (Lakatos et al., 2005b). Thus, it seems that the high-gamma power we recorded from the surface of the cortex is more closely related to neuronal firing than lower frequency bands even in the spontaneous period. However, this conclusion needs to be interpreted with caution because we do not know the exact source of the field potential in our recording from our ECoG arrays. There may be a significant contribution to the high-gamma band power in the field potential recorded at the surface of the cortex from cortical layers other than the superficial layer (Kajikawa and Schroeder, 2011). Also, given the strong correlation between the high-frequency LFP power and sensory BOLD signals (Logothetis et al., 2001), the field potential signals are likely to reflect processes underlying tonotopic maps measured with fMRI (Petkov et al., 2006; Tanji et al., 2010).

Spatiotemporal dynamics of spontaneous activity and its relationship to functional architecture

It has long been clear that spontaneous activity in the cerebral cortex is nonrandom with respect to the layout of the cortical surface: an early set of studies using voltage sensitive dyes combined with optical imaging in the anesthetized cat demonstrated considerable spatial organization in the spontaneous fluctuations of visual cortex (Arieli et al., 1995; 1996). During development, the spontaneous activity became more structured in parallel with the maturation of visual cortex (Fiser et al., 2004; Berkes et al., 2011). The similarity between spontaneous and stimulus-evoked responses has been investigated previously in rodent cortex (Petersen et al., 2003; Poulet and Petersen, 2008; Luczak et al., 2009; Sakata and Harris, 2009). Although these studies found similar temporal dynamics in spontaneous and evoked activity in both anesthetized and, to a limited extent, awake animals (Ferezou et

al., 2007), they have not reported the specific relationship between the sensory map structure derived from evoked activity and that derived from spontaneous activity. Our finding is most similar to a result obtained in an optical imaging study, in which the spatial structure of the orientation map in the primary visual cortex was identified from spontaneous neural activity in anesthetized cats (Kenet et al., 2003). Long-term optical imaging of the visual cortex has also been carried out in awake macaques (Shtoyerman et al., 2000), but the structure of the sensory map was not determined from the spontaneous activity. Thus, our finding opens up the possibility of uncovering the relationship between spontaneous activity and the functional architecture of cortical areas that may not be identifiable in the anesthetized animal.

The functional significance of the structured spontaneous activity we found, such as its effects on neural and behavioral responses to auditory stimuli, has yet to be evaluated. Spontaneous ongoing activity in the inter-stimulus interval has previously been shown to affect sensory responses to stimuli. For example, in visual cortex of the anesthetized cat, a large portion of the stimulus-evoked response variability is linearly explained by the preceding state of spontaneous activity (Arieli et al., 1996). Similarly, in auditory cortex of the anesthetized rat, a nonlinear dynamical model estimated from pre-stimulus spontaneous population activity preceding stimulus presentation explained the trial-to-trial variability of the auditory evoked response (Curto et al., 2009). In auditory cortex of awake macaque, the pre-stimulus low frequency oscillation (delta) phase has an effect on stimulus evoked responses (CSD or multi-unit spikes) (Lakatos et al., 2005b). Moreover, the pre-stimulus delta phase can become non-random as stimuli are presented at a constant rate (Lakatos et al., 2005b). This suggests that an entrainment or adaptive effect of the stimulation history may also be reflected in pre-stimulus spontaneous activity. Pre-stimulus spontaneous EEG activity in humans also predicts the magnitude of fMRI responses to visual stimuli (Becker et al., 2011). Some other evidence suggests that the state of spontaneous activity can also influence the capacity to detect stimuli. Behaviorally, humans are more likely to detect auditory or visual stimuli when the spontaneous fMRI signal is high in the respective sensory cortical areas (Hesselmann et al., 2010). In the visual cortex of behaving macaque monkeys, attention modulates the pre-stimulus low frequency oscillations that affect the visual event-related response (Lakatos et al., 2008). This also suggests that the cognitive and behavioral state of an awake animal may substantially affect the pattern of the spontaneous activity. In light of these findings, it would be interesting to investigate how the behavioral state could modulate the pattern of the spontaneous activity resembling the tonotopic maps.

Although the exact origin of the structured spontaneous activity in the cerebral cortex is not fully understood (Leopold and Maier, 2011), it is likely that anatomical constraints related to functional specialization contributed to the spatiotemporal structure of coherent spontaneous fluctuations among similar frequency sites in our study. This co-modulation would need common input to multiple auditory areas and/or long-range corticocortical connections among those areas. There is well-established anatomical evidence that the three “core” areas (A1, R, and RT) receive thalamic inputs from the ventral nucleus of the medial geniculate complex (Kaas, 2000 for a review). For such thalamic inputs to co-modulate neurons with the same frequency preference across the three areas, the same, or correlated, thalamic neuron(s) would need to terminate within each cortical areas at points with the same frequency preference. To our knowledge, such a frequency specific pattern of thalamic inputs has not been reported. As for corticocortical connection, there are long-range anatomical connections between cortical columns with similar stimulus frequency in the cat auditory cortex (Read et al., 2001; Lee et al., 2004). In the macaque auditory cortex, long range connections also exist between preferred high-frequency sites in A1 and R (Morel et al., 1993). While details of the anatomical connections to and from more rostral auditory areas have not yet been investigated systematically in the macaque, such connections

between sites with similar frequency preference could account for the spontaneous covariation of the sites resembling the tonotopic maps found in this study. It has been theoretically demonstrated that networks of neurons with proper connections can produce spontaneous oscillatory population activity (Wilson and Cowan, 1972; 1973; Amari, 1977; Wallace et al., 2011) and that spontaneous pattern formation in the visual cortex can result from the symmetry in the cortical connections (Bressloff et al., 2001) between cortical columns with similar stimulus preferences (Bosking et al., 1997). In addition, there could be another contribution to the structured spontaneous activity from the corticothalamocortical circuit, which could have a role in signal propagation from primary to higher auditory areas even in absence of corticocortical connections (Theyel et al., 2009).

A rather different, though not mutually exclusive, possibility is that the structured spontaneous activity reflects the playback of information about experienced or learned stimuli. A recent study in the rodent visual cortex holds that, following the repeated presentation of a visual stimulus, spontaneous spatiotemporal activity resembled the evoked activity and persisted in this form for several minutes after the stimulation (Han et al., 2008), raising the possibility of a link to short-term memory. This effect is similar in some respects to our results, but the origin of structured spontaneous activity in our data would be different from such putative short-term memory effects since our recordings of the spontaneous activity were carried out during different sessions and on different days from those in which the sensory evoked responses were mapped. Alternatively, the structured spontaneous activity in our data may reflect auditory information stored in long-term memory (if auditory long-term memory is present in the monkey; (see Fritz et al., 2005). During sleep, the ‘replay’ of learning-related activity has been observed in the rodent hippocampus (Wilson and McNaughton, 1994) and prefrontal cortex (Euston et al., 2007) as well as in the songbird premotor nucleus (Dave and Margoliash, 2000). More recently, replay was also identified in the hippocampus of awake animals (Foster and Wilson, 2006; Carr et al., 2011). Such replay of learning-related activity stored long-term could drive structured spontaneous activity in the sensory cortex (Ji and Wilson, 2006).

In summary, our approach with chronically implanted μECoG arrays allowed us to identify the sensory map and probe the spatiotemporal dynamics of intrasulcal auditory cortical areas in awake monkeys. This led to the finding that spontaneous activity reflected the functional architecture of the auditory cortex along nearly the entire supratemporal plane. The experimental and analytical methods that led to the finding holds promise for advancing our understanding of how the spectral and temporal features of highly complex sounds (Bendor and Wang, 2008), such as species-specific vocalizations (Poremba et al., 2004; Petkov et al., 2008; Kikuchi et al., 2010; Perrodin et al., 2011), are processed in the auditory cortex.

Experimental Procedures

Subjects

Two adult rhesus monkeys (*Macaca mulatta*) weighing 5.5–9 kg were used. All procedures and animal care were conducted in accordance with the Institute of Laboratory Animal Resources Guide for the Care and Use of Laboratory Animals, and under an approved National Institute of Mental Health Animal Care and Use Committee protocol. The monkeys’ hearing ability was examined with distortion product otoacoustic emission (DPOAE); the results suggest that both monkeys had normal to near-normal peripheral hearing binaurally.

Multielectrode array

We custom-designed a micro-electrocorticographic (μECoG) array to record field potentials from macaque auditory cortex (NeuroNexus Technolgies Inc., MI). The array is machine-fabricated on a very thin polyimide film (20 μm). Each array had 32 recording sites, 50 μm in diameter, on a 4 × 8 grid with 1 mm spacing (i.e. 3 × 7 mm rectangular grid).

Surgery

We implanted 4–5 μECoG arrays in each of two monkeys (Monkey M, five arrays in the right hemisphere; Monkey B, four arrays in the left hemisphere). Three of the arrays were placed on the supratemporal plane, a fourth was positioned over the parabelt on the lateral surface of the superior temporal gyrus (STG) adjacent to A1, and, in monkey M, a fifth array was placed on the lateral surface of STG just rostral to the fourth array (data gathered from the lateral-surface arrays are not reported in this paper). Monkeys were fasted for 12 h before surgery and pretreated with an antibiotic (Ditrim, 24% solution, 0.1 ml/kg i.m.). On the day of surgery, the animal was sedated with ketamine (10 mg/kg i.m.) and anesthetized with isoflurane (1–4% to effect). Throughout surgery, vital signs were monitored, including SpO2, and the animal was kept warm with a heating pad and hydrated (Ringer's solution i.v.). Mannitol (30%, 30 cc i.v. over 20 min) was infused to reduce brain volume. Standard sterile neurosurgical procedures were used throughout. A frontotemporal bone flap, extending from the orbit ventrally toward the temporal pole and caudally behind the auditory meatus, was turned and removed. The dura was then opened and reflected ventrally to expose the lateral sulcus. Using a combination of fine forceps and a small glass pipette attached to a vacuum pump, the banks of the lateral sulcus were carefully separated along its caudo-rostral length, as far medially as the circular sulcus. Special care was taken not to harm the pial surface of the supratemporal plane (STP). The most caudal of the three uECoG arrays on the STP was placed first and aimed at area A1 by positioning it just caudal to an (imaginary) extension of the central sulcus and in close proximity to a small bump on the STP, both being markers of A1's approximate location. Each successively more rostral array was then placed immediately adjacent to the previous one to minimize inter-array gaps. The arrays on lateral surface of the STG were placed last. The probe connector attached to each array was initially glued (vetbond) to the skull immediately above the cranial opening. Once all the arrays were in place within the lateral sulcus and on the lateral surface, the dura was carefully closed and the bone flap reattached. Ceramic screws together with bone cement were used to fix the connectors to the skull. The skin was closed in anatomical layers. Postsurgical analgesics were provided as necessary, in consultation with the National Institute of Mental Health veterinarian.

Histology

On completion of the recording sessions and after injection of anatomical tracers as part of a complementary experiment (the injections were made after removing the upper bank of the lateral sulcus and frontoparietal operculum, illustrated in Figure 1C), one monkey (Monkey M) was injected with a lethal dose of sodium pentobarbital and perfused transcardially with saline followed by 4% paraformaldehyde. The brain was blocked in the coronal plane, removed, photographed, cryoprotected through a series of glycerol solutions (Rosene et al., 1986), frozen, and subsequently sectioned in 40-μm slices on a freezing microtome. Special care was taken to ensure the arrays were not disturbed during the processing of the brain. Several 1-in-20 series were collected and then processed using standard immunohistochemical procedures to identify the auditory areas of the supratemporal plane. One series was processed to visualize the calcium binding protein parvalbumin, another, to visualize the neurofilament SMI-32, and a third series was stained with thionine. Each of these series was examined under the microscope, and the boundaries of the auditory areas were plotted in relation to the positions of the uECoG arrays.

Electrophysiological recording and stimulus presentation

During the experiment, the monkey was placed in a double-walled sound attenuating booth (Biocoustics Instruments Inc., MD). We presented auditory stimuli while the monkey sat in a primate chair with its head fixed. We monitored and recorded the monkey's behavioral state through a video camera connected to a PC to ensure that the animal was calm and awake throughout the experiment. The stimuli were generated digitally (200 kHz sampling rate, 24 bit D/A) by the RX6 Multi Function Processor (Tucker Davis Technology Inc., FL). The sound stimuli were presented on a calibrated free-field speaker (Reveal 501A, Tannoy, Scotland, UK) located 50 cm directly in front of the animal's head. The stimuli were tone bursts (100 ms duration, 2-ms cosine rise/fall). In total, 180 different pure-tone stimuli were used (30 frequencies from 100 Hz to 20 kHz equally spaced logarithmically, each presented at 6 equally-spaced intensity levels from 52–87 dB). We presented these stimuli in pseudorandom order with an interstimulus interval of 1 sec. Each stimulus was presented 60 times to Monkey M and 40 times to Monkey B. The auditory evoked potential from each channel of the μECoG array was band-passed between 2 and 500 Hz, digitally sampled with a sampling rate of 1500 Hz, and stored on hard-disk drives. For recording spontaneous neural activity, no auditory stimulus was presented, and the monkey's ears were covered by an ear muff (Premium ear muff 1440, 3M Inc., MN) to minimize acoustic stimulation from noise. We also monitored and video-recorded the monkey's behavior. The monkeys mostly sat quietly and never vocalized. We excluded epochs of the recording during which the monkey moved suddenly or there was any substantial noise. The total duration of spontaneous-activity recording included in the analyses was 49 min for Monkey M and 61 min for Monkey B).

Data Analysis

MATLAB® (The Mathworks Inc., MA) was used for offline analyses of the field potential data. Since there was little significant auditory evoked power above 250 Hz, we low-pass filtered and resampled the data at 500 Hz to speed up the calculations and reduce the amount of memory necessary for the analysis. The field potential data from each site was re-referenced by subtracting the average of all sites within the same array (Kellis et al., 2010). For the analysis of frequency tuning, the field potential was bandpass filtered in the following conventionally defined frequency ranges: theta (4–8Hz), alpha (8–13 Hz), beta (13–30 Hz), low-gamma (30–60 Hz), and high-gamma (60–200 Hz) (Leopold et al., 2003; Edwards et al., 2005). We filtered the field potential with a butterworth filter. We achieved a zero-phase shift by processing the data in both forward and reverse direction ('filtfilt' function in Matlab). We then computed power in each frequency band in time windows of 150 ms. The power was computed by squaring bandpassed voltage values at each point in time and averaging them for all the points in the 150 ms time window (Figure 2B).

To judge whether the power of the evoked potential from each site significantly discriminated the frequency of the stimulus, we used a two-way ANOVA where the two independent variables were the frequency and intensity of the tone stimulus. A site was defined as 'frequency-tuned' if it had a significant main effect of the stimulus frequency with $p < 0.01$. For frequency-tuned sites, we computed the characteristic frequency (CF) with the power of the evoked field potentials. CF is defined as the frequency that evoked a significant response (t-test, $p < 0.01$ compared to the power from the pre-stimulus presentation period), at the lowest intensity of the stimulus that evoked a significant response. If more than two stimulus frequencies produced significant responses, we defined CF as the mean of the significant frequencies weighted by the power of the responses (Recanzone et al., 2000). The CF values projected on the caudorostal axis were fitted by a polynomial function with a least squares regression ('regress' function in Matlab). The n^{th} order polynomial is defined as follows:

$$f(x)=\sum_{i=0}^{n} a_i x^i$$

The coefficient a_i was determined by the regression from the data.

We calculated the Pearson correlation coefficient between the CF map and each time frame over the entire session of spontaneous activity. The distribution of the correlation coefficient was fitted by a Gaussian that minimized the least squares error. To create the control distribution, we randomized the spatial structure of the CF map and then computed the correlation coefficient. We created 10 different randomized CF maps, and all of the correlation coefficients were used to produce the control distribution.

We used principal component analysis (PCA) to analyze the structure of the correlations in the high-gamma spontaneous activity. The high-gamma band voltage at each of the 96 points along the STP was analyzed over time. The high-gamma band voltage is obtained by band-passing raw voltage between 60–200Hz in spontaneous activity (Figure 4A). Each time point was considered one observation. These were used to calculate a 96 by 96 correlation matrix, which was subjected to PCA. This yielded 96 principal components (PCs) ranked by the amount of the variance explained. Each PC is an eigenvector of the covariance matrix, which corresponds to a spatial mode of the spontaneous activity. For computing PCs, we used ‘princomp’ function in Matlab.

We evaluated whether each PC was correlated with the CF and/or the area label with a general linear model where the dependent variable was the elements of the PC and the independent variables were CF (continuous variable) and the area label (categorical variable). The CF for each site was calculated as described above (see also Figure 3), and sites without significant frequency tuning were not included in the correlation analysis. The area label was assigned to each site based on the areal boundary derived from the tonotopic map in Figure 3 (e.g. 1 for Sector 1, 2 for Sector 2, etc.). As we tested all 96 PCs, the significance level was Bonferroni corrected to 0.05/96.

Supplementary Material

Refer to Web version on PubMed Central for supplementary material.

Acknowledgments

We thank K King for audiologic evaluation of the monkeys’ peripheral hearing, R Reoli, W Wu, A Mitz, B Scott, D Yu, P Leccese, M Mullarkey, J Hollingsworth, and L Kibiuk for technical assistance, D Rickrode, D Jones, and M Manion for animal care, K Saleem, S Guderian, Y Kikuchi, A Maier, M Schmidt, K Tanji, and J Fritz for discussions. This study utilized the high-performance computational capabilities of the Helix Systems (http://helix.nih.gov) and the Biowulf Linux cluster (http://biowulf.nih.gov) at the National Institutes of Health, Bethesda, MD. This research was supported by the Intramural Research Program of the NIH, National Institute of Mental Health (NIMH).

References

Amari S. Dynamics of pattern formation in lateral-inhibition type neural fields. Biol Cybern. 1977; 27:77–87. [PubMed: 911931]

Arieli A, Shoham D, Hildesheim R, Grinvald A. Coherent spatiotemporal patterns of ongoing activity revealed by real-time optical imaging coupled with single-unit recording in the cat visual cortex. J Neurophysiol. 1995; 73:2072–2093. [PubMed: 7623099]

Arieli A, Sterkin A, Grinvald A, Aertsen A. Dynamics of ongoing activity: explanation of the large variability in evoked cortical responses. Science. 1996; 273:1868–1871. [PubMed: 8791593]

Baumann S, Griffiths TD, Rees A, Hunter D, Sun L, Thiele A. Characterisation of the BOLD response time course at different levels of the auditory pathway in non-human primates. NeuroImage. 2010; 50:1099–1108. [PubMed: 20053384]

Becker R, Reinacher M, Freyer F, Villringer A, Ritter P. How Ongoing Neuronal Oscillations Account for Evoked fMRI Variability. J Neurosci. 2011; 31:11016–11027. [PubMed: 21795550]

Bendor D, Wang X. Neural response properties of primary, rostral, and rostrotemporal core fields in the auditory cortex of marmoset monkeys. J Neurophysiol. 2008; 100:888–906. [PubMed: 18525020]

Berkes P, Orbán G, Lengyel M, Fiser J. Spontaneous cortical activity reveals hallmarks of an optimal internal model of the environment. Science. 2011; 331:83–87. [PubMed: 21212356]

Biswal B, Yetkin FZ, Haughton VM, Hyde JS. Functional connectivity in the motor cortex of resting human brain using echo-planar MRI. Magn Reson Med. 1995; 34:537–541. [PubMed: 8524021]

Bolhuis JJ, Okanoya K, Scharff C. Twitter evolution: converging mechanisms in birdsong and human speech. 2010:1–13.

Bosking WH, Zhang Y, Schofield B, Fitzpatrick D. Orientation selectivity and the arrangement of horizontal connections in tree shrew striate cortex. The Journal of Neuroscience. 1997; 17:2112–2127. [PubMed: 9045738]

Bressloff PC, Cowan JD, Golubitsky M, Thomas PJ, Wiener MC. Geometric visual hallucinations, Euclidean symmetry and the functional architecture of striate cortex. Philos Trans R Soc Lond, B, Biol Sci. 2001; 356:299–330. [PubMed: 11316482]

Carr MF, Jadhav SP, Frank LM. Hippocampal replay in the awake state: a potential substrate for memory consolidation and retrieval. Nat Neurosci. 2011; 14:147–153. [PubMed: 21270783]

Chandrasekaran C, Ghazanfar AA. Different Neural Frequency Bands Integrate Faces and Voices Differently in the Superior Temporal Sulcus. J Neurophysiol. 2008; 101:773–788. [PubMed: 19036867]

Chen L, Mishra A, Newton AT, Morgan VL, Stringer EA, Rogers BP, Gore JC. Fine-scale functional connectivity in somatosensory cortex revealed by high-resolution fMRI. Magnetic Resonance Imaging. 2011:1–8.

Crowe DA, Averbeck BB, Chafee MV. Rapid sequences of population activity patterns dynamically encode task-critical spatial information in parietal cortex. J Neurosci. 2010; 30:11640–11653. [PubMed: 20810885]

Curto C, Sakata S, Marguet S, Itskov V, Harris KD. A Simple Model of Cortical Dynamics Explains Variability and State Dependence of Sensory Responses in Urethane-Anesthetized Auditory Cortex. J Neurosci. 2009; 29:10600–10612. [PubMed: 19710313]

Da Costa S, van der Zwaag W, Marques JP, Frackowiak RSJ, Clarke S, Saenz M. Human Primary Auditory Cortex Follows the Shape of Heschl's Gyrus. J Neurosci. 2011; 31:14067–14075. [PubMed: 21976491]

Dave AS, Margoliash D. Song replay during sleep and computational rules for sensorimotor vocal learning. Science. 2000; 290:812–816. [PubMed: 11052946]

Edwards E, Soltani M, Deouell LY, Berger MS, Knight RT. High gamma activity in response to deviant auditory stimuli recorded directly from human cortex. J Neurophysiol. 2005; 94:4269–4280. [PubMed: 16093343]

Euston DR, Tatsuno M, McNaughton BL. Fast-Forward Playback of Recent Memory Sequences in Prefrontal Cortex During Sleep. Science. 2007; 318:1147–1150. [PubMed: 18006749]

Ferezou I, Haiss F, Gentet L, Aronoff R, Weber B, Petersen C. Spatiotemporal dynamics of cortical sensorimotor integration in behaving mice. Neuron. 2007; 56:907–923. [PubMed: 18054865]

Fiser J, Chiu C, Weliky M. Small modulation of ongoing cortical dynamics by sensory input during natural vision. Nature. 2004; 431:573–578. [PubMed: 15457262]

Fishman YI, Steinschneider M. Neural correlates of auditory scene analysis based on inharmonicity in monkey primary auditory cortex. J Neurosci. 2010; 30:12480–12494. [PubMed: 20844143]

Formisano E, Kim D, Di Salle F, van de Moortele P, Ugurbil K, Goebel R. Mirror-symmetric tonotopic maps in human primary auditory cortex. Neuron. 2003; 40:859–869. [PubMed: 14622588]

Foster DJ, Wilson MA. Reverse replay of behavioural sequences in hippocampal place cells during the awake state. Nature. 2006; 440:680–683. [PubMed: 16474382]

Fritz J, Mishkin M, Saunders R. In search of an auditory engram. P Natl Acad Sci Usa. 2005; 102:9359–9364.

Fu KMG. Timing and Laminar Profile of Eye-Position Effects on Auditory Responses in Primate Auditory Cortex. J Neurophysiol. 2004; 92:3522–3531. [PubMed: 15282263]

Hackett TA. Information flow in the auditory cortical network. Hear Res. 2011; 271:133–146. [PubMed: 20116421]

Han F, Caporale N, Dan Y. Reverberation of Recent Visual Experience in Spontaneous Cortical Waves. Neuron. 2008; 60:321–327. [PubMed: 18957223]

He BJ, Snyder AZ, Zempel JM, Smyth MD, Raichle ME. Electrophysiological correlates of the brain's intrinsic large-scale functional architecture. Proceedings of the National Academy of Sciences. 2008; 105:16039–16044.

Hesselmann G, Sadaghiani S, Friston KJ, Kleinschmidt A. Predictive Coding or Evidence Accumulation? False Inference and Neuronal Fluctuations. PLoS ONE. 2010; 5:e9926. [PubMed: 20369004]

Huang X, Troy W, Yang Q, Ma H, Laing C, Schiff S, Wu J. Spiral waves in disinhibited mammalian neocortex. J Neurosci. 2004; 24:9897–9902. [PubMed: 15525774]

Ji D, Wilson MA. Coordinated memory replay in the visual cortex and hippocampus during sleep. Nat Neurosci. 2006; 10:100–107. [PubMed: 17173043]

Kaas JH. Subdivisions of auditory cortex and processing streams in primates. Proceedings of the National Academy of Sciences. 2000; 97:11793–11799.

Kajikawa Y, Schroeder CE. How Local Is the Local Field Potential? Neuron. 2011; 72:847–858. [PubMed: 22153379]

Kayser C, Montemurro MA, Logothetis NK, Panzeri S. Spike-Phase Coding Boosts and Stabilizes Information Carried by Spatial and Temporal Spike Patterns. Neuron. 2009; 61:597–608. [PubMed: 19249279]

Kayser C, Petkov CI, Logothetis NK. Tuning to Sound Frequency in Auditory Field Potentials. J Neurophysiol. 2007; 98:1806–1809. [PubMed: 17596418]

Kellis S, Miller K, Thomson K, Brown R, House P, Greger B. Decoding spoken words using local field potentials recorded from the cortical surface. J Neural Eng. 2010; 7:056007. [PubMed: 20811093]

Kenet T, Bibitchkov D, Tsodyks M, Grinvald A, Arieli A. Spontaneously emerging cortical representations of visual attributes. Nature. 2003; 425:954–956. [PubMed: 14586468]

Kennedy C, Sakurada O, Shinohara M, Jehle J, Sokoloff L. Local cerebral glucose utilization in the normal conscious macaque monkey. Ann Neurol. 1978; 4:293–301. [PubMed: 103488]

Kikuchi Y, Horwitz B, Mishkin M. Hierarchical auditory processing directed rostrally along the monkey's supratemporal plane. J Neurosci. 2010; 30:13021–13030. [PubMed: 20881120]

Kim J, Wilson JA, Williams JC. A cortical recording platform utilizing microECoG electrode arrays. Conference Proceedings: Annual International Conference of the IEEE Engineering in Medicine and Biology Society IEEE Engineering in Medicine and Biology Society Conference. 2007; 2007:5353–5357. [PubMed: 18003217]

Kusmierek P, Rauschecker JP. Functional specialization of medial auditory belt cortex in the alert rhesus monkey. J Neurophysiol. 2009; 102:1606–1622. [PubMed: 19571201]

Lakatos P, Karmos G, Mehta AD, Ulbert I, Schroeder CE. Entrainment of neuronal oscillations as a mechanism of attentional selection. Science. 2008; 320:110–113. [PubMed: 18388295]

Lakatos P, Pincze Z, Fu KMG, Javitt DC, Karmos G, Schroeder CE. Timing of pure tone and noise-evoked responses in macaque auditory cortex. Neuroreport. 2005a; 16:933–937. [PubMed: 15931064]

Lakatos P, Shah AS, Knuth KH, Ulbert I, Karmos G, Schroeder CE. An oscillatory hierarchy controlling neuronal excitability and stimulus processing in the auditory cortex. J Neurophysiol. 2005b; 94:1904–1911. [PubMed: 15901760]

Lee CC, Schreiner CE, IMAIZUMI K, Winer JA. Tonotopic and heterotopic projection systems in physiologically defined auditory cortex. Nsc. 2004; 128:871–887.

Lee D, Port NL, Kruse W, Georgopoulos AP. Variability and correlated noise in the discharge of neurons in motor and parietal areas of the primate cortex. The Journal of Neuroscience. 1998; 18:1161–1170. [PubMed: 9437036]

Leopold D, Murayama Y, Logothetis N. Very slow activity fluctuations in monkey visual cortex: implications for functional brain imaging. Cereb Cortex. 2003; 13:422–433. [PubMed: 12631571]

Leopold DA, Logothetis NK. Spatial patterns of spontaneous local field activity in the monkey visual cortex. Rev Neurosci. 2003; 14:195–205. [PubMed: 12929926]

Leopold DA, Maier A. Ongoing physiological processes in the cerebral cortex. NeuroImage. 2011:1–11.

Liu J, Newsome WT. Local field potential in cortical area MT: stimulus tuning and behavioral correlations. J Neurosci. 2006; 26:7779–7790. [PubMed: 16870724]

Logothetis N, Pauls J, Augath M, Trinath T, Oeltermann A. Neurophysiological investigation of the basis of the fMRI signal. Nature. 2001; 412:150–157. [PubMed: 11449264]

Luczak A, Barthó P, Harris KD. Spontaneous Events Outline the Realm of Possible Sensory Responses in Neocortical Populations. Neuron. 2009; 62:413–425. [PubMed: 19447096]

Merzenich MM, Brugge JF. Representation of the cochlear partition of the superior temporal plane of the macaque monkey. Brain Res. 1973; 50:275–296. [PubMed: 4196192]

Morel A, Garraghty PE, Kaas JH. Tonotopic organization, architectonic fields, and connections of auditory cortex in macaque monkeys. J Comp Neurol. 1993; 335:437–459. [PubMed: 7693772]

Ogawa T, Riera J, Goto T, Sumiyoshi A, Nonaka H, Jerbi K, Bertrand O, Kawashima R. Large-Scale Heterogeneous Representation of Sound Attributes in Rat Primary Auditory Cortex: From Unit Activity to Population Dynamics. J Neurosci. 2011; 31:14639–14653. [PubMed: 21994380]

Perrodin C, Kayser C, Logothetis NK, Petkov CI. Voice Cells in the Primate Temporal Lobe. Current Biology. 2011; 21:1408–1415. [PubMed: 21835625]

Petersen CCH, Grinvald A, Sakmann B. Spatiotemporal dynamics of sensory responses in layer 2/3 of rat barrel cortex measured in vivo by voltage-sensitive dye imaging combined with whole-cell voltage recordings and neuron reconstructions. J Neurosci. 2003; 23:1298–1309. [PubMed: 12598618]

Petkov CI, Kayser C, Augath M, Logothetis NK. Functional Imaging Reveals Numerous Fields in the Monkey Auditory Cortex. PLoS Biol. 2006; 4:e215. [PubMed: 16774452]

Petkov CI, Kayser C, Steudel T, Whittingstall K, Augath M, Logothetis NK. A voice region in the monkey brain (supplementary materials). Nat Neurosci. 2008:1–7. [PubMed: 18160952]

Poremba A, Malloy M, Saunders R, Carson R, Herscovitch P, Mishkin M. Species-specific calls evoke asymmetric activity in the monkey's temporal poles. Nature. 2004; 427:448–451. [PubMed: 14749833]

Poulet JFA, Petersen CCH. Internal brain state regulates membrane potential synchrony in barrel cortex of behaving mice. Nature. 2008; 454:881–885. [PubMed: 18633351]

Raichle ME, MacLeod AM, Snyder AZ, Powers WJ, Gusnard DA, Shulman GL. A default mode of brain function. P Natl Acad Sci Usa. 2001; 98:676–682.

Rauschecker JP, Tian B, Hauser M. Processing of complex sounds in the macaque nonprimary auditory cortex. Science. 1995; 268:111–114. [PubMed: 7701330]

Ray S, Crone NE, Niebur E, Franaszczuk PJ, Hsiao SS. Neural correlates of high-gamma oscillations (60–200 Hz) in macaque local field potentials and their potential implications in electrocorticography. J Neurosci. 2008; 28:11526–11536. [PubMed: 18987189]

Read HL, Winer JA, Schreiner CE. Modular organization of intrinsic connections associated with spectral tuning in cat auditory cortex. P Natl Acad Sci Usa. 2001; 98:8042–8047.

Recanzone GH, Guard DC, Phan ML. Frequency and intensity response properties of single neurons in the auditory cortex of the behaving macaque monkey. J Neurophysiol. 2000; 83:2315–2331. [PubMed: 10758136]

Rosene DL, Roy NJ, Davis BJ. A cryoprotection method that facilitates cutting frozen sections of whole monkey brains for histological and histochemical processing without freezing artifact. Journal of Histochemistry & Cytochemistry. 1986; 34:1301–1315. [PubMed: 3745909]

Sakata S, Harris KD. Laminar structure of spontaneous and sensory-evoked population activity in auditory cortex. Neuron. 2009; 64:404–418. [PubMed: 19914188]

Scott BH, Malone BJ, Semple MN. Transformation of temporal processing across auditory cortex of awake macaques. J Neurophysiol. 2011; 105:712–730. [PubMed: 21106896]

Shtoyerman E, Arieli A, Slovin H, Vanzetta I, Grinvald A. Long-term optical imaging and spectroscopy reveal mechanisms underlying the intrinsic signal and stability of cortical maps in V1 of behaving monkeys. The Journal of Neuroscience. 2000; 20:8111. [PubMed: 11050133]

Steinschneider M, Fishman YI, Arezzo JC. Spectrotemporal analysis of evoked and induced electroencephalographic responses in primary auditory cortex (A1) of the awake monkey. Cereb Cortex. 2008; 18:610–625. [PubMed: 17586604]

Tanji K, Leopold DA, Ye FQ, Zhu C, Malloy M, Saunders RC, Mishkin M. Effect of sound intensity on tonotopic fMRI maps in the unanesthetized monkey. NeuroImage. 2010; 49:150–157. [PubMed: 19631273]

Theyel BB, Llano DA, Sherman SM. The corticothalamocortical circuit drives higher-order cortex in the mouse. Nat Neurosci. 2009; 13:84–88. [PubMed: 19966840]

Tsodyks M, Kenet T, Grinvald A, Arieli A. Linking spontaneous activity of single cortical neurons and the underlying functional architecture. Science. 1999; 286:1943. [PubMed: 10583955]

Wallace E, Benayoun M, van Drongelen W, Cowan JD. Emergent oscillations in networks of stochastic spiking neurons. PLoS ONE. 2011; 6:e14804. [PubMed: 21573105]

Wilson HR, Cowan JD. Excitatory and inhibitory interactions in localized populations of model neurons. Biophysical Journal. 1972; 12:1–24. [PubMed: 4332108]

Wilson HR, Cowan JD. A mathematical theory of the functional dynamics of cortical and thalamic nervous tissue. Kybernetik. 1973; 13:55–80. [PubMed: 4767470]

Wilson MA, McNaughton BL. Reactivation of hippocampal ensemble memories during sleep. Science. 1994; 265:676–679. [PubMed: 8036517]

Wu JY, Huang X, Zhang C. Propagating Waves of Activity in the Neocortex: What They Are, What They Do. Neuroscientist. 2008; 14:487–502. [PubMed: 18997124]

Xu W, Huang X, Takagaki K, Wu JY. Compression and reflection of visually evoked cortical waves. Neuron. 2007; 55:119–129. [PubMed: 17610821]

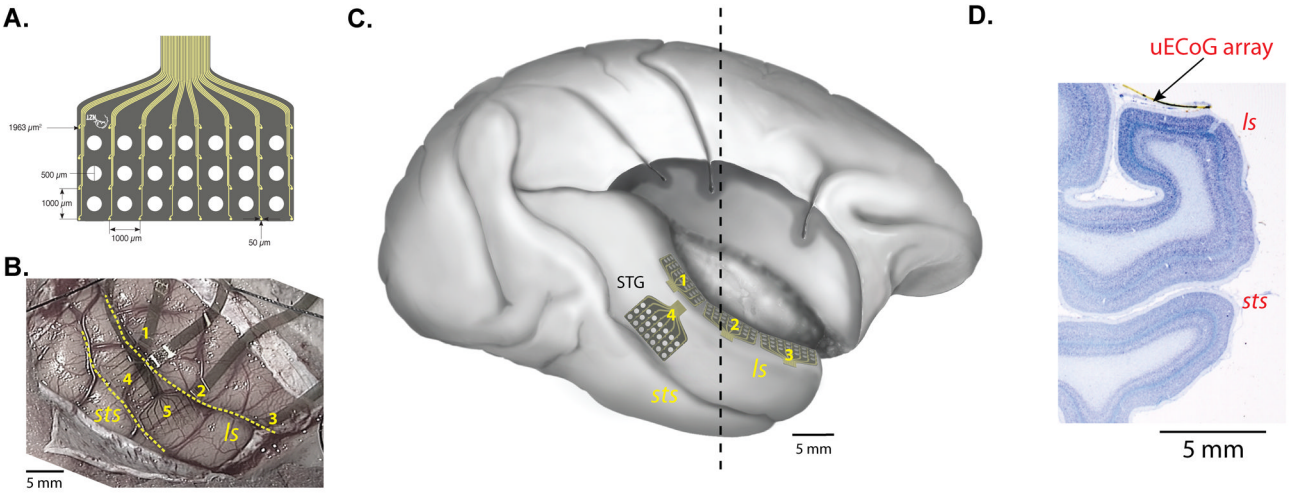

Figure 1.

Micro-electrocorticographic (μECoG) arrays and implanted locations. **A.** μECoG array designed for this study (figure courtesy of Neuronexus Inc.) consists of 32 electrodes in a 4 × 8 pattern (small yellow dots) fabricated on a 20-μm thick polyimide film. The large white circles are holes in the array designed for microinjections. **B.** Implanted locations of five arrays (numbered 1–5) in Monkey M. Three arrays (1, 2, and 3) were inserted in the lateral sulcus and positioned on the supratemporal plane. The two other arrays were placed on the lateral surface of the superior temporal gyrus. **C.** Lateral view of the right hemisphere reproduced from the postmortem brain of Monkey M after removing the upper bank of the lateral sulcus and frontoparietal operculum to visualize the location of the three arrays (1–3) on the supratemporal plane, on which we focused in the current study. 5th array is not drawn in this figure. **D.** Nissl-stained coronal section taken from the approximate location of the dashed line in **C.** The brain was serially sectioned with the implanted array in place; a piece of the array is visible on the STP in this section. Abbreviations: *ls*, lateral sulcus; STP, supratemporal plane; *sts,* superior temporal sulcus.

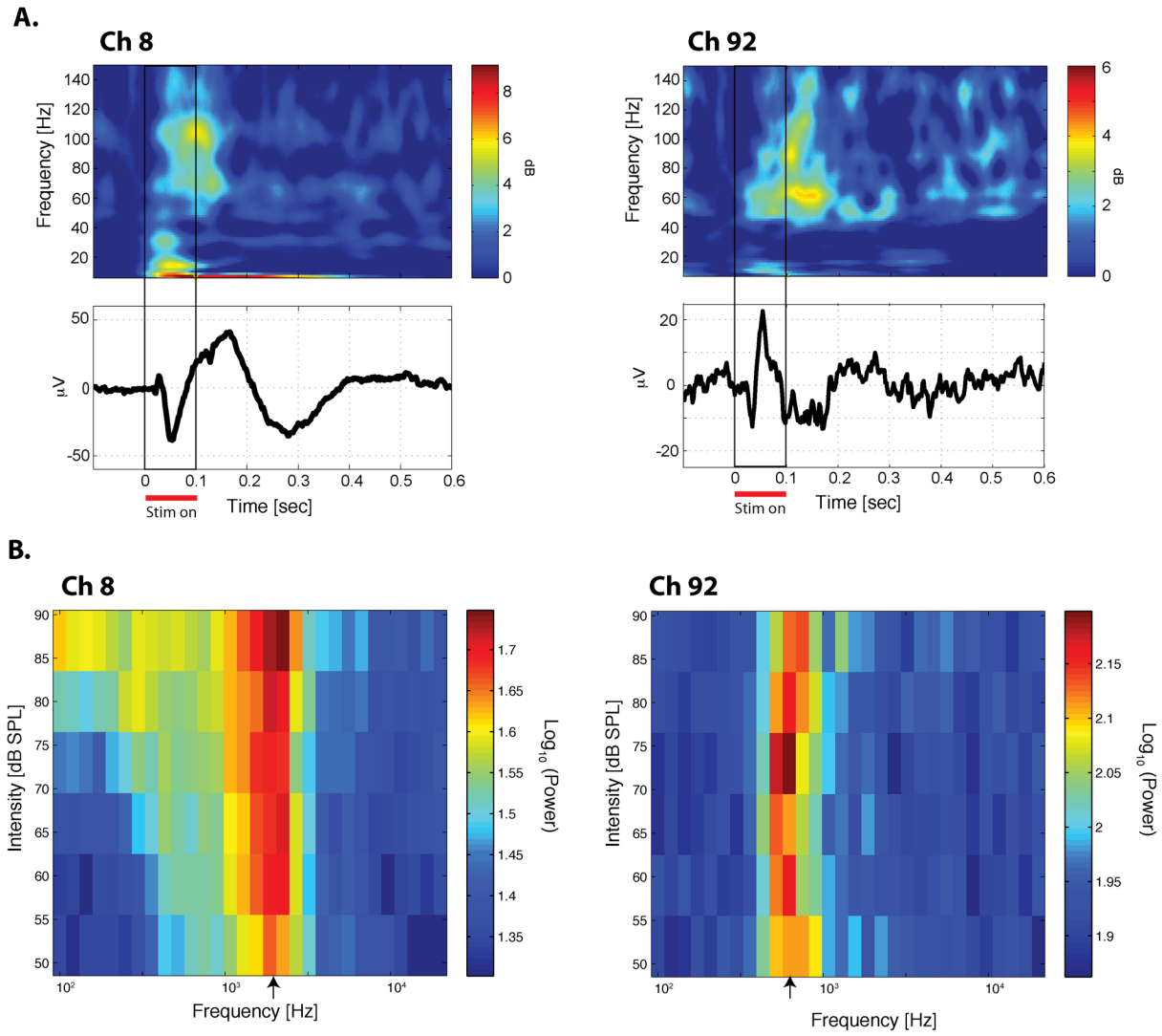

Figure 2. Examples of the auditory evoked potential and the characteristic frequency

A. Upper panels: trial-averaged spectrograms to a tone stimulus. The spectrograms were normalized by the prestimulus-period activity. **Lower panels:** trial-averaged auditory evoked potential to the same tone stimulus in Upper panel. Left panels from Ch 8 in the most caudal array; Right pannels from Ch 92 in the most rostral array, both from Monkey M). **B.** Frequency-intensity tuning curve. The average evoked high-gamma power from the first 150 ms is plotted for each of the 180 tone stimuli (30 frequencies × 6 intensity levels). The unit of power is $(\mu V)^2$. The log (base 10) of the power is color-coded. The characteristic frequency (CF) is indicated by the arrow on the frequency axis. See also Figure S3 for supplemental information for this figure.

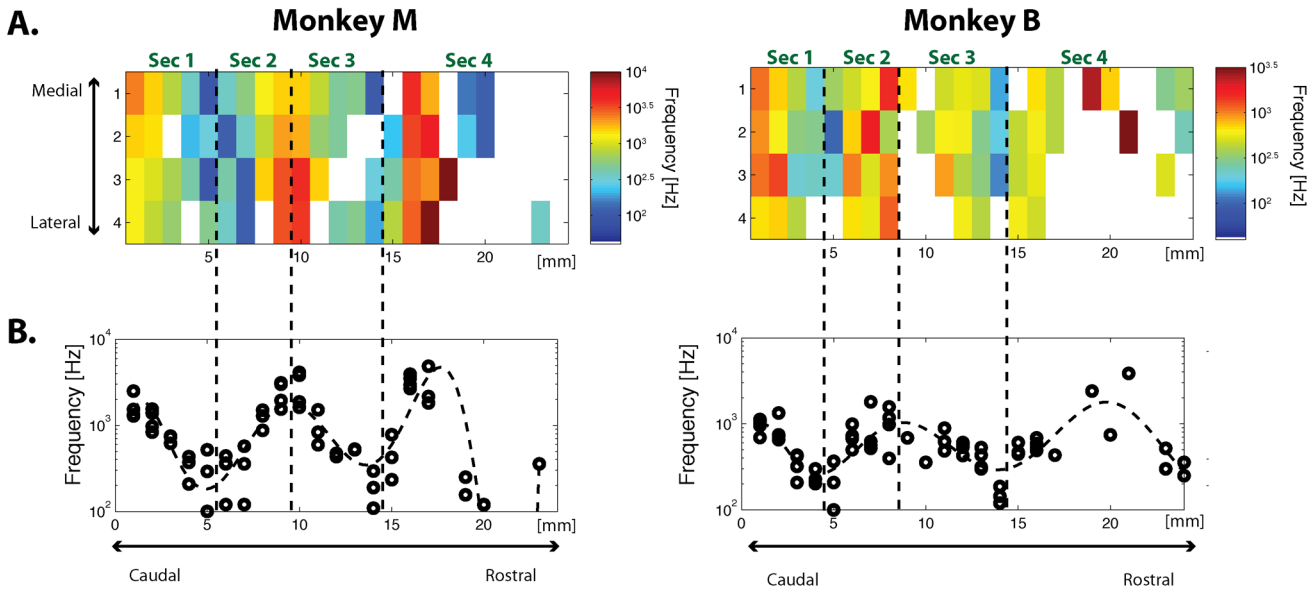

Figure 3. Tonotopic map on the STP obtained with high-gamma power

A. The spatial map of the estimated CFs for each monkey (Left: Monkey M; Right: Monkey B). The CFs are color coded. White indicates site without significant frequency tuning. **B.** The CFs projected onto their caudorostral locations. Each CF from **A** is plotted on the vertical axis and its corresponding caudorostral location is plotted on the horizontal axis. Abbreviation: Sec, Sector (see main text for definition of each sector). (See also Figure S3 and Table S1 for supplemental information for this figure.)

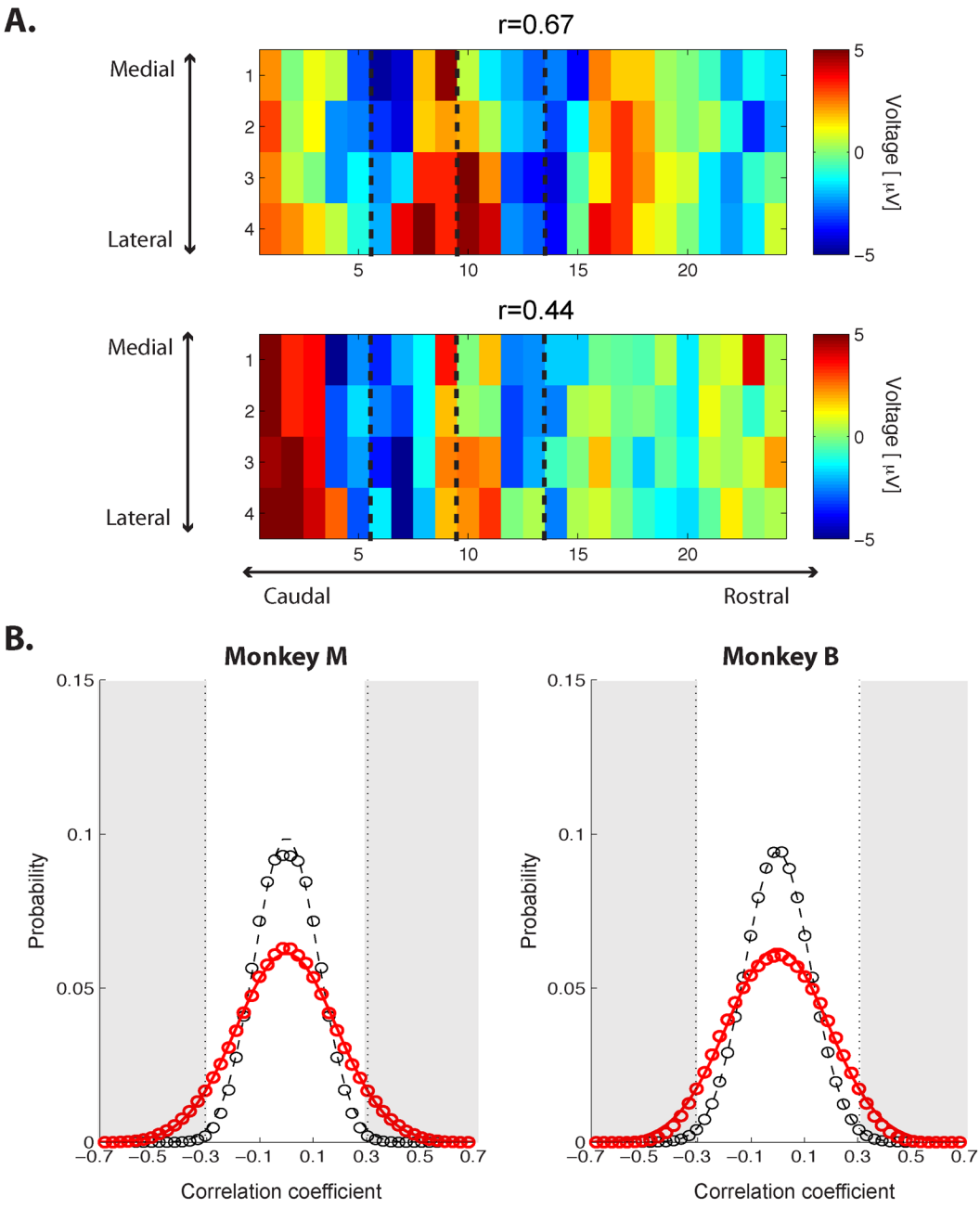

Figure 4. The spatial structure of the spontaneous high-gamma band voltage is correlated with the CF map

A. Two time frames from spontaneous high-gamma voltage illustrating the significant correlations between spontaneous activity and the CF map (Monkey M: Top, r = 0.67; Bottom, r = 0.44). The dashed lines indicates the boundaries of different sectors as defined in Figure 3A. **B.** Distributions of correlation between the CF map and spontaneous activity (Left: Monkey M, Right: Monkey B). Red, the distribution of correlation coefficients between the CF map and spontaneous-voltage time frames over the entire recording session. Black, the control distribution created by correlating with randomized CF maps (with 10 different randomizations). Each distribution was fitted by a Gaussian, indicated by the lines. The significance level was computed from the control distribution for $p < 0.01$ (two-sided, p

< 0.005 on each side). The gray area indicates the correlation coefficients satisfying this significance level.

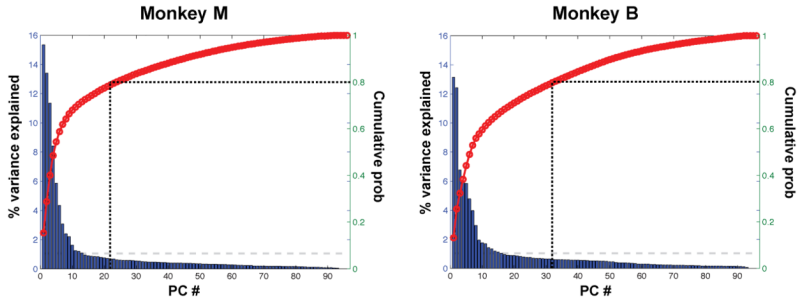

Figure 5. The amount of variance explained by each principal component from the spontaneous activity

(Left: Monkey M, Right: Monkey B). Bar plot with the ordinate labeling on the left side:The percentage of variance explained by each principal component. Red curve with the ordinate labeling on the right side: The cumulative probability of the variance explained. The vertical dotted line indicates the number of principal components necessary to explain 80% of the total variance of the data (22 for Monkey M, 32 for Monkey B). The gray dashed line indicates the percentage of variance explained by uniformly distributed eigen values.

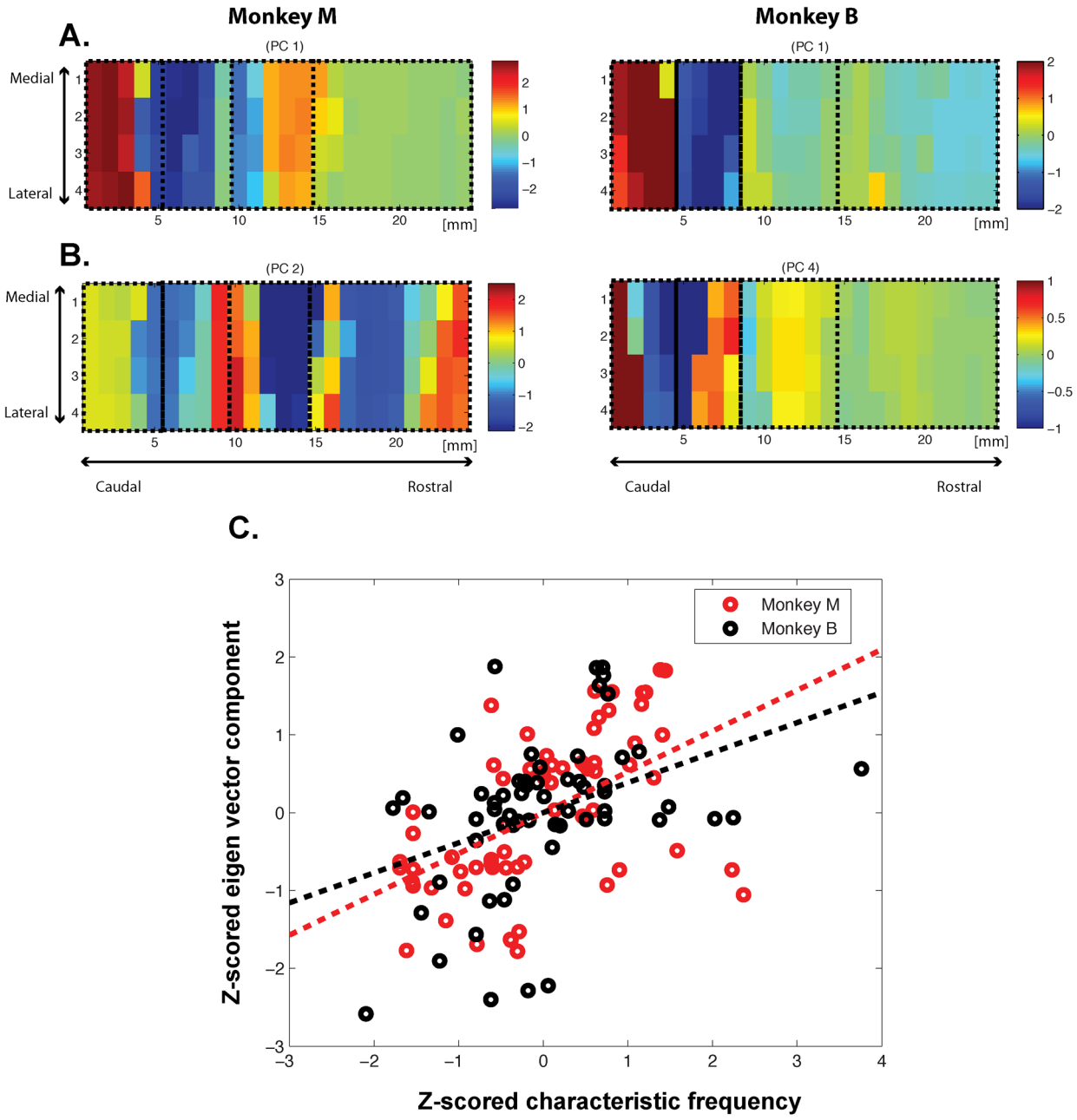

Figure 6. Principal components from the spontaneous activity correlated with the functional architecture of the auditory cortex

A. The highest-order PCs that correlated with the areal map. The first PCs provide the eigenvector with the highest correlation for both Monkey M (left) and Monkey B (right). **B.** The highest-order PCs that correlated with the tonotopic map. The second PC for Monkey M (left) and the fourth PC for Monkey B (right). **C.** the scatter plot showing the correlation between the normalized CFs and eigenvalues plotted in B for significant frequency-tuned sites in Figure 3A. Each circle corresponds to one of the significantly tuned site. (See also Figure S2 and Table S2 for supplemental information for this figure.)